A Dual-Layer Receiver With a Low Aspect Ratio and a Reduced Output Fluctuation for EV Dynamic Wireless Charging

Beibei Song, Shuai Dong, Yong Li, and Shumei Cui

***Abstract*—A dual-layer receiver with a low aspect ratio and a low output fluctuation is proposed in this article. It is composed of three parts: full-pitch coils, mixed-pitch coils, and a flat receiver core. In EV dynamic wireless charging system, power supply rails with alternately arranged poles, such as I-type, S-type, and N-type rails, have the advantage of narrow width, but they also show the main drawback of sinusoidal output fluctuation when they are mated with conventional double D (DD) receiver coils. To solve this problem, a dual-layer receiver is proposed in this article. Through the combination of full-pitch coils and mixed-pitch coils, the output fluctuation factor can be reduced from 100% to 29%. Compared with the conventional dual-DD receiver, the proposed receiver shows the following advantages. Full-pitch and mixed-pitch coils are not required to be dislocated in space so that the aspect ratio is reduced by 20%. In this way, the problems of too large receiver size and limited installation space can be solved, and the cross coupling between the receiver coils can be eliminated as well. Based on the theoretical analysis of the working principle of the dual-layer receiver, the output voltage expression of receiver coils is derived and the basic relationship between full-pitch and mixed-pitch coils is explored. Then, the influences of the mixed-pitch coil's symmetry and vehicle chassis on the system are analyzed, and the design principle of the proposed receiver is given. In addition, the dual-layer receiver is extended to multiple receivers through multiple cascades to further reduce the output fluctuation factor. Finally, a 10-kW prototype with ac–dc efficiency of 93.2% was built for experimental verification. The experimental results were consistent with theoretical analysis and simulation results, thus proving that the proposed receiver could reduce the aspect ratio and achieve the decoupling between the receiver coils under the premise of reducing the output fluctuation.**

***Index Terms*—Dual-layer receiver, dynamic wireless charging (DWC), EV, low aspect ratio, low output fluctuation.**

I. Introduction

EVS can effectively alleviate the problems of environmental pollution and energy shortage. However, the disadvantages of EVs such as insufficient driving range and frequent parking charging have greatly limited their application scope [1]. The dynamic wireless charging (DWC) technology can solve the above problems well [2]. This technology not only greatly increases the driving range of vehicles, but also largely reduces the weight of on-board batteries. In addition, the dynamic charging mode can effectively reduce the waiting time of parking charging and avoid the deep charge and discharge of the battery, thus improving the health management and service life of batteries [3]–[5].

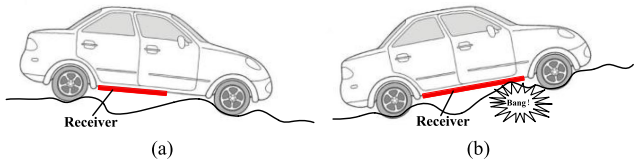

Fig. 1. Influence of receiver's aspect ratio on vehicle's off-road performance. (a) Low aspect ratio. (b) High aspect ratio.

In the DWC system, power supply rails with alternately arranged poles, such as I-type, S-type, and N-type rails, have been widely applied due to their advantages of narrow width and strong lateral displacement capability [6]–[8]. However, these power supply rails have a common drawback: when they are mated with conventional double D (DD) receiver coils, the output voltage has a sinusoidal variation during the driving process, and reaches zero at a specific position. A larger output fluctuation not only reduces the average output power of the system, but also increases the harmonic amplitude of the receiver's dc output voltage, thus further increasing the design difficulty of the receiver converter. Therefore, it is necessary to reduce the output fluctuation. Moreover, the installation space of the chassis is limited for EVs. In order to ensure the off-road performance of EVs, the length of the on-board receiver should be reduced and the aspect ratio should be as low as possible to avoid chassis bumping during the climbing process, as shown in Fig. 1.

Reducing the output power fluctuation is a key problem to be urgently solved in the DWC technology for EVs. At present, there are three mainstream solutions. The first solution is to use multiple receivers. Dual and quadruple receivers were, respectively, proposed [9], [10]. Through different connection modes between multiple receivers, the output fluctuation factors of dual and quadruple receivers were reduced to 0.3 and 0.146, respectively. However, the two receivers had the shortcomings of high aspect ratio and long receiver size, so their application scope was limited by the chassis installation space. A dual-layer

Manuscript received January 19, 2020; accepted February 28, 2020. Date of publication March 4, 2020; date of current version June 23, 2020. This work was supported by the National Natural Science Foundation of China under Grant 51577034. Recommended for publication by Associate Editor R. Hui. *(Corresponding author: Shuai Dong.)*

The authors are with the School of Electrical Engineering and Automation, Harbin Institute of Technology, Harbin 150001, China (e-mail: songbei_mt@126.com; dongshuai@hit.edu.cn; liyong611@hit.edu.cn; cuism@hit.edu.cn).

Color versions of one or more of the figures in this article are available online at http://ieeexplore.ieee.org.

Digital Object Identifier 10.1109/TPEL.2020.2978214

DDQ receiver [8] was proposed to reduce the output fluctuation through the connection of DD coils and Q coil after rectification. However, the number of turns of the Q coil needs to be two times or more than that of the DD coils, thus resulting in too large voltage stress of the Q coil and the coil insulation problem. At the same time, limited by the winding space of the Q coil, this receiver is only suitable for applications with few coil turns and low output power.

The second solution is to use multiphase transmitters. Three kinds of three-phase magnetic couplers with different structures were proposed [11]–[14]. A two-phase magnetic coupler with *dq*-power supply rails was also proposed [15]. The above structures can theoretically achieve the uniform output power through the traveling wave magnetic field generated by multiphase transmitter coils. However, for magnetic couplers with multiphase transmitters, the wire amount of transmitter coils is large and the design of inverter is complicated. In addition, the cross coupling between multiphase transmitter coils increases the cost and control difficulty of the system.

The third solution is to use the system control strategy. Two different control strategies for array transmitter coils were proposed to reduce the output power fluctuation by controlling the turn-ON time and the switching sequence of adjacent multiple transmitter coils [16], [17]. A control strategy for rectangular array transmitter coils [18] was proposed to reduce the output fluctuation by sequentially turning ON the adjacent two transmitter coils, which had the highest coupling degree with the receiver. However, the above system control strategies require the position detection device, so the system's detection and control technology is complex and the reliability is low.

In summary, the multiphase transmitter solution has the disadvantage of high cost, whereas the circuit control solution has the disadvantages of complicated control and low reliability. In contrast, the multireceiver solution has the advantages of high reliability, low cost, and huge engineering potential. At present, the most important limitation factors of multireceiver solution are the high aspect ratio and the limited chassis installation space. These factors are explored in this article.

This article proposes a dual-layer receiver with a low output fluctuation, a low aspect ratio, and a low chassis occupancy. The proposed receiver consists of three parts: full-pitch coils, mixed-pitch coils, and a flat ferrite core. Through the arrangement of different lengths of each coil in the mixed-pitch coils, the output voltages of the full-pitch coils and the mixed-pitch coils maintain a spatial phase difference of 90° along the driving direction without displacement. In this way, the load voltage will pulse twice during the vehicle's travel through a pole pitch, thereby avoiding power zero and reducing output fluctuation. Compared with the coils in conventional dual DD-type receivers, the full-pitch and mixed-pitch coils in the proposed receiver are spatially overlapped to reduce the receiver's aspect ratio and the space occupation ratio of the chassis. Compared with the conventional DDQ-type receivers, the proposed receiver reduces the turns of the Q coil by adding two short coils in the mixed-pitch coils, and solves the problems of limited winding space and difficult coil insulation of the Q coil.

The remainder of this article is organized as follows. In Section II, the configuration and working principle of the dual-layer receiver are proposed, and the new receiver is compared with the conventional dual-DD-type receiver. In Section III, the design of the proposed receiver is given, and the system efficiency and the influence of vehicle chassis on the magnetic coupler are analyzed. In Section IV, a prototype with an output power of 10.64 kW and ac–dc efficiency of 93.2% was built for experimental verification. Finally, Section V concludes this article.

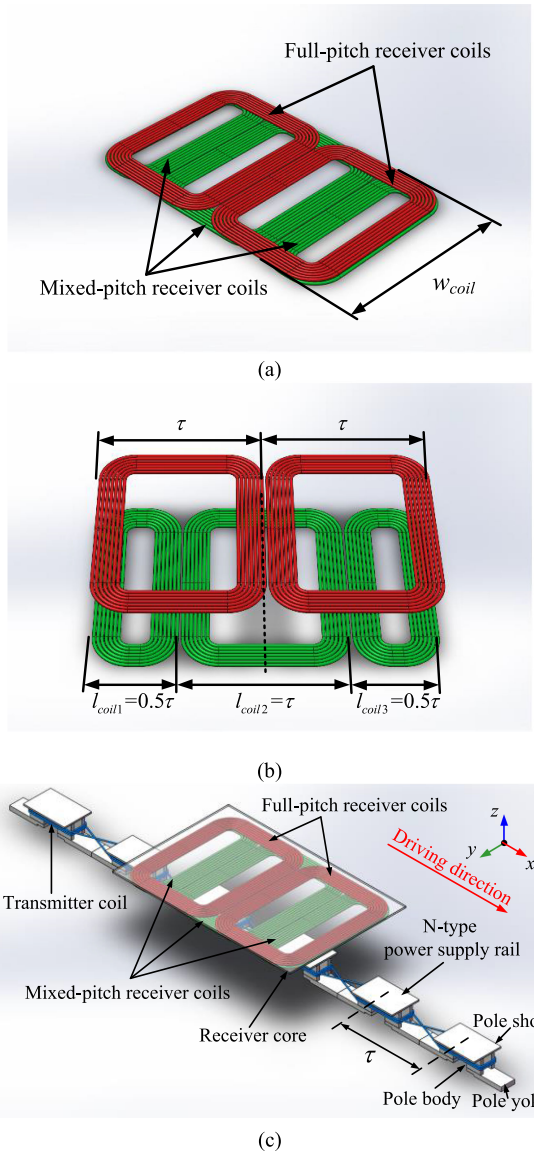

Fig. 2. Structure diagram of the proposed dual-layer receiver. (a) Bird view. (b) Main view. (c) Schematic diagram of the receiver when mated with N-type power supply rail.

II. Configuration and Working Principle

A. Configuration of the Proposed Receiver

The dual-layer receiver used in the DWC system for EVs is shown in Fig. 2. The receiver consists of three parts: full-pitch receiver coils, mixed-pitch receiver coils, and a flat ferrite core. The flat core is laid directly above the receiver coils and can be used to improve mutual inductance and coupling coefficient, and

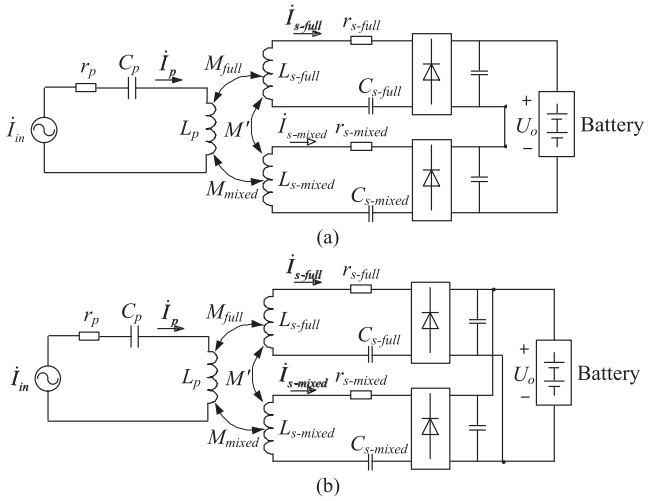

Fig. 3. Circuit diagram of the system. (a) Series connection. (b) Parallel connection.

shield the leakage magnetic field generated from the magnetic coupler to the vehicle chassis.

As shown in Fig. 2(a) and (b), the full-pitch receiver coils consist of two DD coils connected in series. Each coil has a width of w_{coil} and a length of τ. Since the coil lengths of both DD coils are equal to pole pitch τ of the power supply rail, the receiver coils are called full-pitch coils. The mixed-pitch receiver coils consist of three rectangular coils (denoted as coil_1, coil_2, and coil_3) connected in series, and every two adjacent coils are wound in opposite directions. Coil widths are the same as that of the full-pitch coils, whereas coil lengths are 0.5τ, τ, and 0.5τ, respectively. Since the receiver coils are composed of coils with different lengths, the receiver coils are called mixed-pitch coils. The total length of the receiver coils is 2τ and the numbers of turns of all coils in the two sets of coils are the same.

In terms of the spatial relative position, full-pitch and mixed-pitch receiver coils are overlapped in the vertical direction. Compared with the coils of conventional multiple receivers [9], [10], the full-pitch and mixed-pitch coils in the proposed receiver do not need to be spatially displaced along the driving direction, thereby greatly reducing the aspect ratio of the receiver and the space occupation ratio of the chassis.

In terms of the circuit connection, full-pitch and mixed-pitch receiver coils are rectified to supply power to the on-board battery, respectively. As shown in Fig. 3(a) and (b), they can be connected in series or parallel after rectification. In Fig. 3, r_p and L_p, respectively, indicate the internal resistance and self-inductance of the transmitter coil and C_p and I_p, respectively, indicate the resonant capacitor and the current in the transmitter coil. Similarly, the corresponding parameters of the full-pitch and mixed-pitch coils are, respectively, indicated as $r_{s-\text{full}}$, $r_{s-\text{mixed}}$, $L_{s-\text{full}}$, $L_{s-\text{mixed}}$, $C_{s-\text{full}}$, $C_{s-\text{mixed}}$, $I_{s-\text{full}}$, and $I_{s-\text{mixed}}$, whereas M_{full} and M_{mixed}, respectively, indicate the mutual inductance between the transmitter coil and the two sets of receiver coils. M' represents the cross coupling between the full-pitch and mixed-pitch coils. For the proposed receiver, M' is zero since the mixed-pitch coils are designed to be decoupled from the full-pitch coils. The decoupling design is discussed in Section III.

B. Working Principle

The proposed dual-layer receiver is mated with power supply rails with alternately arranged poles, such as I-type, S-type, and N-type rails. When the receiver is mated with the N-type power supply rail, the structure diagram is shown in Fig. 2(c). The output power fluctuation is reduced by maintaining the two sets of receiver coils' output voltage with the receiver position x at a spatial phase difference of 90° along the driving direction.

When the receiver is mated with power supply rails with alternately arranged poles, the mutual inductance M between a single rectangular receiver coil and the transmitter coil varies approximately sinusoidally with the receiver position x [15]. The relationship between M and x is expressed as

$$M = M_{\max} \cdot \sin\left(\frac{\pi}{\tau}x\right) \tag{1}$$

where $M_{\max}$ indicates the magnitude of the mutual inductance. The mutual inductance M reaches its maximum value when the receiver coil is located directly above the magnetic pole, and drops to zero when the receiver coil is located directly above the central line of two adjacent poles. In this article, $x = 0$ is defined as the position when coil_2 in the mixed-pitch coils is located above the magnetic pole.

To simplify the analysis, this article uses the concept of an electrical angle to represent the length of the receiver coil. A pair of magnetic poles in the power supply rail is defined to correspond to an electrical angle of 360°. Then, the relationship between the pole pitch τ and the electrical angle satisfies the following equation:

$$2\tau = 360^\circ. \tag{2}$$

In the full-pitch receiver coils, the electrical angle of each DD coil is 180°. Since the winding directions of two DD coils are opposite, the mutual inductance M_{full} between the full-pitch coils and the transmitter coil satisfies

$$\begin{aligned} M_{\text{full}} &= M_{\pi-\max} \cdot \sin\left(\frac{\pi}{\tau}x\right) - M_{\pi-\max} \cdot \sin\left(\frac{\pi}{\tau}x + \pi\right) \\ &= 2M_{\pi-\max} \cdot \sin\left(\frac{\pi}{\tau}x\right) \end{aligned} \tag{3}$$

where $M_{\pi-\max}$ indicates the magnitude of the mutual inductance between a D coil and the transmitter coil. For the mixed-pitch receiver coils, the electrical angles of coil_1, coil_2, and coil_3 are α, β, and α, respectively. Since the total length of the mixed-pitch coils is 2τ, α and β satisfy

$$2\alpha + \beta = 360^\circ \tag{4}$$

According to the relative position relationship between the full-pitch and the mixed-pitch coils shown in Fig. 2(b), the mutual inductances between the three coils in mixed-pitch coils and the transmitter coil can be expressed in (5) and the corresponding curves are shown in Fig. 4(a)

$$\begin{cases} M_{\text{coil1}} = M_{\alpha-\max} \cdot \sin\left(\frac{\pi}{\tau}x - \frac{\pi}{2} + \frac{\alpha}{2}\right) \\ M_{\text{coil2}} = M_{\beta-\max} \cdot \sin\left(\frac{\pi}{\tau}x - \frac{\pi}{2}\right) \\ M_{\text{coil3}} = M_{\alpha-\max} \cdot \sin\left(\frac{\pi}{\tau}x - \frac{\pi}{2} - \frac{\alpha}{2}\right) \end{cases} \tag{5}$$

where $M_{\alpha-\max}$ and $M_{\beta-\max}$ are the mutual inductance amplitudes between the transmitter coil and each receiver coil in the

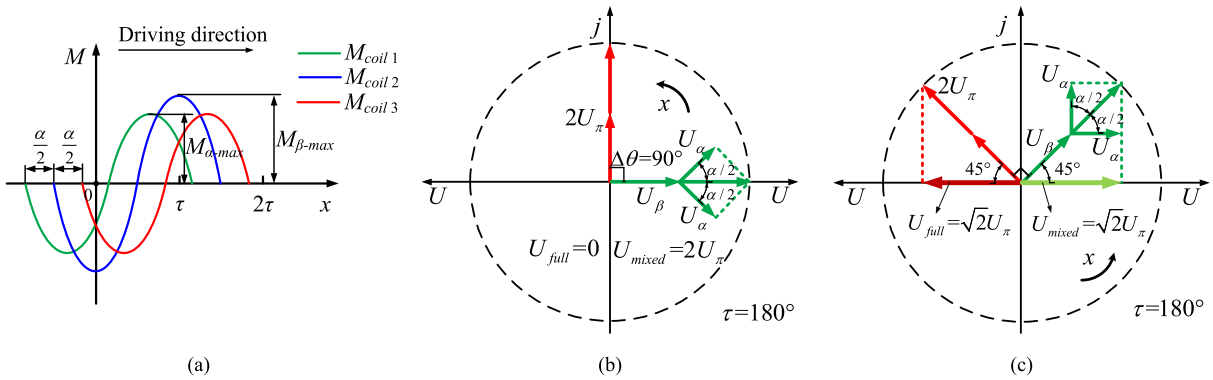

Fig. 4. Phasor diagrams of induced voltages' rms values in the two sets of receiver coils versus receiver's position x. (a) Mutual inductance versus receiver's position x. (b) Phasor diagram of induced voltages when $x = 0$. (c) Phasor diagram of induced voltage when $x = 0.25\tau$.

mixed-pitch coils, respectively. The magnitudes are related to the coil size, the core structure, and the coil's relative position, and will be analyzed in Section III.

The mutual inductance M_{mixed} between the mixed-pitch coils and the transmitter coil is the algebraic sum of M_{coil1}, M_{coil2}, and M_{coil3} and can be simplified as

$$M_{\text{mixed}} = (2M_{\alpha-\max} \cdot \cos\frac{\alpha}{2} + M_{\beta-\max}) \cdot \sin\left(\frac{\pi}{\tau}x - \frac{\pi}{2}\right). \tag{6}$$

The dual-layer receiver is symmetrical and there is no cross coupling between the full-pitch coils and the mixed-pitch coils. Therefore, the two sets of receiver coils' voltages are only induced by the transmitter coil. Through a reasonable design, the amplitudes of the mutual inductance between the transmitter coil and two sets of receiver coils are the same and satisfy the following equation:

$$2M_{\pi-\max} = 2M_{\alpha-\max} \cdot \cos\frac{\alpha}{2} + M_{\beta-\max}. \tag{7}$$

Then, the induced voltages generated in the two sets of coils $\dot{U}_{\text{full}}$ and $\dot{U}_{\text{mixed}}$ are expressed as follows:

$$\begin{cases} \dot{U}_{\text{full}} = 2j\omega\dot{I}_p M_{\pi-\max} \cdot \sin\left(\frac{\pi}{\tau}x\right) \\ \dot{U}_{\text{mixed}} = 2j\omega\dot{I}_p M_{\pi-\max} \cdot \sin\left(\frac{\pi}{\tau}x - \frac{\pi}{2}\right). \end{cases} \tag{8}$$

It can be seen from the above equation that $\dot{U}_{\text{full}}$ and $\dot{U}_{\text{mixed}}$ maintain a spatial phase difference 90° along the driving direction. When $x = 0$ and $x = 0.25\ \tau$, the phasor diagrams of the induced voltages' rms values in the two sets of coils (denoted as U_{full} and U_{mixed}) are shown in Fig. 4(b) and (c), respectively. In Fig. 4, the projection of the voltage phasor on the x-axis is used to represent the rms value of the induced voltage.

From Fig. 4, we can draw the following conclusions. First, as the receiver moves along the driving direction, the rms value of induced voltages in coil_1 and coil_3 (denoted as U_α) and the rms value of the induced voltage in coil_2 (denoted as U_β) maintain a spatial phase difference of $\pm\alpha/2$, respectively, and U_{full} and U_{mixed} always maintain a spatial phase difference of 90°. Second, when $x = k\tau$, U_{mixed} reaches the maximum value, U_{full} drops to 0, and when $x = k\tau \pm 0.5\tau$, the opposite is true. Third, when $x = k\tau \pm 0.25\tau$, U_{full} is equal to U_{mixed}.

When the coil's internal resistance is ignored, rectifier output voltages of the full-pitch coils, the mixed-pitch coils, and their

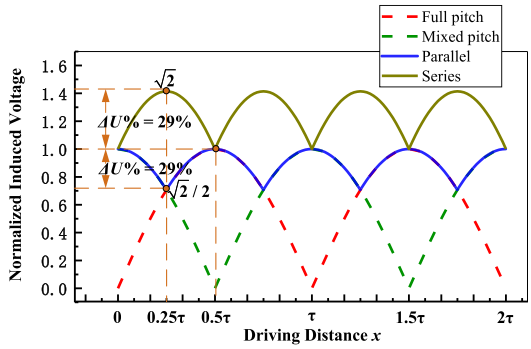

Fig. 5. Rectifier output voltages versus receiver's position x.

different connection modes are shown in Fig. 5. In the figure, $\Delta U\%$ represents the output fluctuation factor and defined as

$$\Delta U\% = \frac{U_{\max} - U_{\min}}{U_{\max}} \times 100\%. \tag{9}$$

As shown in Fig. 5, compared with the conventional dual-DD receiver coils, the proposed receiver can reduce the output fluctuation factor $\Delta U\%$ from 100% to 29% by connecting full-pitch and mixed-pitch receiver coils in series or parallel after rectification. In this way, the output stability is significantly improved. The connection mode of the two sets of receiver coils only affects the amplitude of the output voltage, but it does not affect the output fluctuation factor $\Delta U\%$.

When the two sets of coils are connected in parallel after rectification, only the set with a higher rms value of induced voltage is working, whereas the other set does not turn ON due to the reverse blocking of a rectifier diode. As the receiver moves, the two sets of coils work alternately and the maximum output voltage is equal to the output voltage amplitude of a single set of coils. The average output power during the DWC process is

$$\begin{aligned} \bar{P}_{o-p} &= \frac{1}{\tau}\int_0^\tau \frac{\left(\frac{\pi}{2\sqrt{2}} \cdot \omega \cdot I_p \cdot \max(|M_{\text{full}}|, |M_{\text{mixed}}|)\right)^2 dx}{R_L} \\ &= \frac{\pi^2\omega^2 I_p^2 M_{\pi-\max}^2}{4R_L}\left(1 + \frac{2}{\pi}\right) \end{aligned} \tag{10}$$

where R_L indicates the equivalent resistance of the battery.

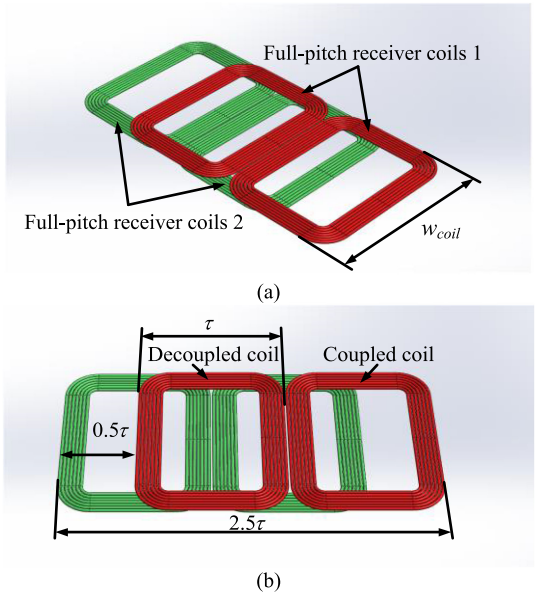

Fig. 6. Schematic diagram of the conventional dual-DD receiver. (a) Bird view. (b) Main view.

When the two sets of coils are connected in series after rectification, both of them turn ON at the same time. The output voltage is equal to the sum of the two sets of coils' output voltages and the maximum value is $\sqrt{2}$ times of the amplitude of a single set of coils. As the receiver moves, the average output power during the DWC process is expressed as

$$\begin{aligned}\bar{P}_{o-s} &= \frac{1}{\tau}\int_{.0}^{\tau}\frac{\left(\frac{\pi}{2\sqrt{2}}\cdot\omega\cdot I_p\cdot\left(|M_{\text{full}}|+|M_{\text{mixed}}|\right)\right)^2 dx}{R_L} \\ &= \frac{\pi^2\omega^2 I_p^2 M_{\pi-\max}^2}{4R_L}\left(2+\frac{4}{\pi}\right). \end{aligned} \tag{11}$$

According to (10) and (11), the output power of series connection mode is twice of the parallel connection mode. In order to obtain the same output power, the parallel connection mode requires the higher current in the transmitter coil, thus increasing the loss of transmitter. However, the parallel connection mode can avoid the influence of cross coupling between the two sets of receiver coils on the output, whereas the series connection mode cannot avoid it [10]. For the proposed receiver, there is no cross coupling between the two sets of coils. Therefore, the series connection mode is more suitable since the higher output power can be obtained.

C. Comparison With Conventional Dual-DD Receivers

The proposed receiver is compared with the conventional dual-DD receiver in terms of aspect ratio, output fluctuation, output power amplitude and cross coupling between receiver coils. A conventional dual-DD receiver (see Fig. 6) is composed of two identical full-pitch coils. For the convenience of comparison, the parameters such as the size, the number of turns, and the wire diameter of full-pitch coils are the same in the proposed and conventional receivers.

In the conventional dual-DD receiver, the *U–x* curves of the two full-pitch coils should maintain a spatial phase difference of 90° to reduce the output fluctuation factor. Therefore, two sets of coils should be placed at an offset distance of 0.5τ along the driving direction. During the dynamic charging process, induced voltages in two sets of receiver coils satisfy

$$\begin{cases}\dot{U}_{\text{full}-1} = 2j\omega\dot{I}_p M_{\text{DD}-\max}\cdot\sin\left(\frac{\pi}{\tau}x\right) \\ \dot{U}_{\text{full}-2} = 2j\omega\dot{I}_p M_{\text{DD}-\max}\cdot\sin\left(\frac{\pi}{\tau}x-\frac{\pi}{2}\right).\end{cases} \tag{12}$$

In terms of the aspect ratio, the total length of the receiver coils in the conventional dual-DD receiver is 2.5τ and the width is w_{coil}. Therefore, the aspect ratio $\lambda_{\text{conventional}}$ is

$$\lambda_{\text{conventional}} = \frac{2.5\tau}{w_{\text{coil}}}. \tag{13}$$

In the proposed receiver, the full-pitch coils or the mixed-pitch coils need not to be misplaced, so the total length of the coils is only 2τ. Since the width remains unchanged, the corresponding aspect ratio $\lambda_{\text{proposed}}$ is

$$\lambda_{\text{proposed}} = \frac{2\tau}{w_{\text{coil}}}. \tag{14}$$

According to (13) and (14), the aspect ratio of the proposed receiver is 20% lower than that of the conventional one. It can reduce the space occupation ratio of the chassis and improve the off-road performance of the vehicle. In addition, it can also reduce the amount of receiver ferrite cores. Therefore, the cost and self-weight of the on-board receiver can be decreased.

In terms of the output fluctuation, *U–x* curve of the proposed receiver is exactly the same as that of the conventional dual-DD receiver. Therefore, their output fluctuation factors $\Delta U\%$ are both 29%.

In terms of the output power amplitude, since the size of full-pitch coils are the same, mutual inductance amplitudes between the transmitter coil and the full-pitch coils in the two structures are the same, indicating that $M_{\text{DD}-\max} = M_{\pi-\max}$. According to (8) and (12), the output power amplitudes of two receivers are the same.

In terms of the cross coupling between receiver coils, there is no cross coupling between the two sets of coils in the proposed receiver. However, in the conventional dual-DD receiver, two full-pitch coils are coupled with each other. As shown in Fig. 6(b), the full-pitch receiver coils 1 (the red part) is composed of a decoupled coil and a coupled coil. The decoupled coil is orthogonal to the other full-pitch receiver coils (the green part), whereas the coupled coil is coupled with the other full-pitch receiver coils.

Therefore, in engineering applications, the conventional dual-DD receiver requires an additional decoupling inductance to eliminate the cross coupling between the two sets of receiver coils [19]. Otherwise, the energy transfer exists between the receiver coils, thus increasing the reactive power of the system and reducing the output power amplitude. However, the additional decoupling inductance will bring out the following problems. First, the cost and weight of the receiver are increased. Second, the self-inductance and internal resistance of receiver coils are increased, thus resulting in the higher voltage stress of the resonance capacitor and the lower coil-to-coil efficiency. Third, the precious installation space in the vehicle is occupied and it is difficult to shield the generated electromagnetic radiation.

TABLE I
COMPARISON BETWEEN THE PROPOSED RECEIVER AND CONVENTIONAL DUAL-DD RECEIVER

Structures	Aspect ratio λ	Receiver length	Cross Coupling	Fluctuation factor $\triangle U\%$	Average output power(Series-connection)
Conventional	$\frac{2.5\tau}{w_{Pu}}$	2.5τ	Existent	29%	$\frac{\pi^2\omega^2 I_p^2 M^2_{\pi-max}}{4R_L}(2+\frac{4}{\pi})$
Proposed	$\frac{2\tau}{w_{Pu}}$	2τ	Non-existent	29%	$\frac{\pi^2\omega^2 I_p^2 M^2_{\pi-max}}{4R_L}(2+\frac{4}{\pi})$

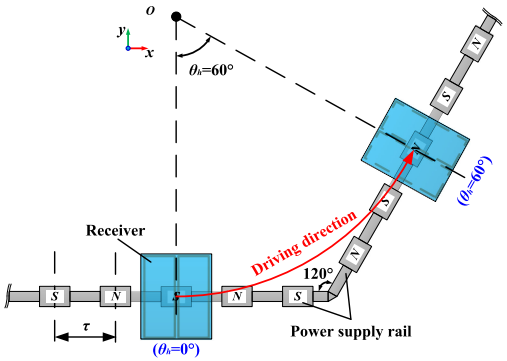

Fig. 7. Electric vehicle turning diagram.

TABLE II
PARAMETERS OF SIMULATION MODEL

Parameters	Symbols	Values	Parameters	Symbols	Values
Air gap	h	200 mm	Pole pitch	τ	600 mm
Pole shoe length	l_b	300 mm	Pole body length	l_m	300 mm
Pole shoe width	w_b	200 mm	Pole body width	w_m	100 mm
Pole shoe thickness	t_b	10 mm	Pole body height	h_m	100 mm
Pole yoke width	w_j	100 mm	Receiver core length	l_{core}	1300 mm
Pole yoke thickness	t_j	30 mm	Receiver core width	w_{core}	800 mm
Receiver coil width	w_{coil}	800 mm	Receiver core thickness	t_{core}	10 mm
Number of turns of transmitter coil	N_P	4	Number of turns of receiver coil	N_S	5

In the proposed receiver, there is no cross coupling between the mixed-pitch coils and the full-pitch coils. Therefore, the proposed receiver can avoid the above problems.

The comparison between the proposed dual-layer receiver and the conventional dual-DD receiver is provided in Table I.

D. Output Fluctuation During Vehicle Turning

In engineering applications, it is necessary to consider the situation of vehicle turning. Fig. 7 shows the relative position relationship between the receiver and the power supply rail during the vehicle turning process. The angle between the two power supply rails is 120° and the driving track of the receiver center is shown in the red arc. During the vehicle turning process, the receiver is misaligned and deflected, and the angle between the receiver and the power supply rail is also changed.

The mutual inductance between the transmitter coil and each receiver coils during the vehicle turning process was obtained through finite element simulation. The parameters of the simulation model are as listed in Table II.

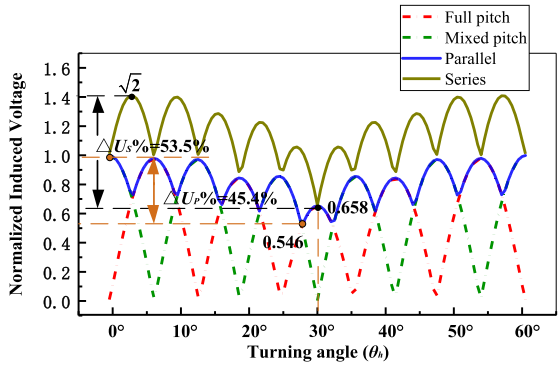

Fig. 8. Rectifier output voltages versus turning angle θ_h.

Based on the simulation results, the relationship between the rectifier output voltage and the turning angle θ_h is obtained (see Fig. 8).

The results in Fig. 8 are summarized as follows. First, when the vehicle drives on a straight road, the output voltage fluctuation is 29%. During the turning process, the output voltage fluctuations of series and parallel connection modes are, respectively, increased to 53.5% and 45.4%. Second, the output voltages of full-pitch coils and mixed-pitch coils first decrease and then increase with the increase in the turning angle θ_h and the minimum value occurs when $\theta_h = 30°$. However, both sets of receiver coils still maintain the same output amplitude. Third, the output fluctuation factors of both connection modes are not the same any more and the parallel connection mode has a lower voltage fluctuation factor.

In summary, during the vehicle turning process, though the output voltage fluctuation increases compared with that obtained under the straight-line driving conditions, the proposed receiver can avoid zero output. In engineering applications, the DWC should be mainly concentrated on the straight-line driving conditions, and the turning process is generally so short. Thus, the increase in the output fluctuation caused by vehicle turning has little effect on the overall charging process of the system.

E. Extension of the Proposed Receiver

For vehicles with a large chassis installation space such as electric buses, the proposed dual-layer receiver can be extended to be multiple receivers through multiple connections so as to further reduce the output fluctuation factor. The structure diagram of the quadruple receiver extended from two proposed dual-layer receivers is shown in Fig. 9(a).

The quadruple receiver consists of two proposed receivers spaced apart by 2.75 τ along the driving direction and the two receivers have a spatial phase difference of 135°. Since there is a distance of 0.75 τ between two receivers, the cross coupling between them can be ignored. According to (8), the rectified output voltages of two sets of full-pitch coils and two sets of mixed-pitch coils in the quadruple receiver have a spatial phase difference of 45° along the driving direction. Therefore, when the receiver moves the distance of a pole pitch τ, the load output voltage U_o pulses four times, so that the output fluctuation factor can be further reduced. When the internal resistance of the

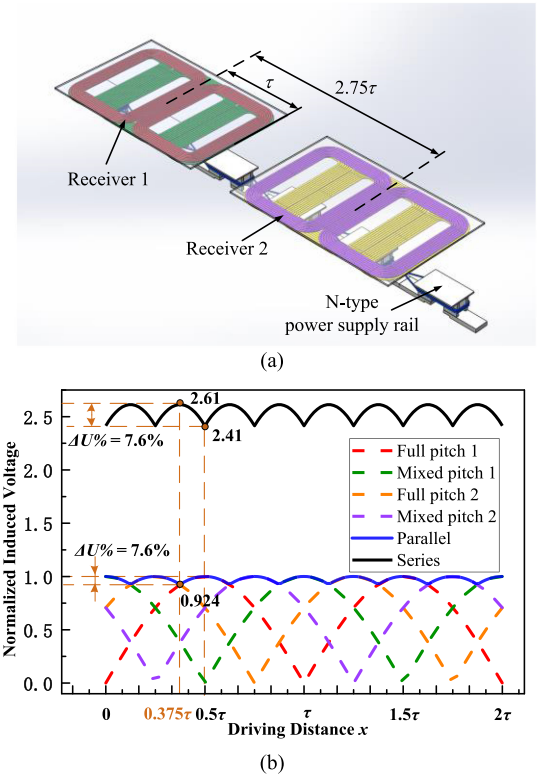

Fig. 9. Quadruple receiver extended from two proposed receivers. (a) Schematic diagram of the quadruple receiver. (b) Rectifier output voltages versus receiver's position x.

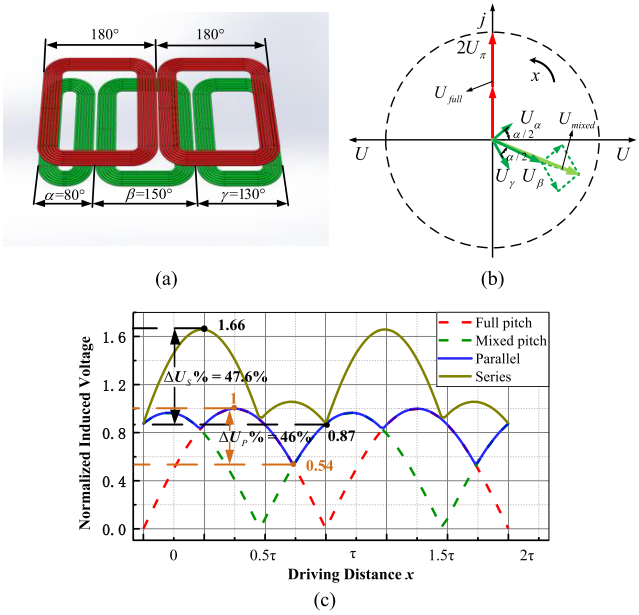

Fig. 10. Asymmetrical dual-layer receiver. (a) Structure diagram of the asymmetrical receiver. (b) Phasor diagram of the induced voltages when $x = 0$. (c) Rectifier output voltages versus receiver's position x.

receiver coil is ignored, the output voltage curves (U–x curve) of the quadruple receiver in different connection modes shown in Fig. 9(b) can be obtained.

As shown in Fig. 9, the quadruple receiver can further reduce the output fluctuation factor $\Delta U\%$ from 29% to 7.6%, indicating that the output fluctuation can be significantly decreased. Similarly, the output fluctuations of both series connection mode and parallel connection mode are the same.

For the quadruple receiver extended from two proposed dual-layer receivers, the total length is 4.75 τ and the aspect ratio λ is: 4.75 τ/w_{coil}. As for the quadruple receiver [10] extended from conventional dual-DD receivers, the total length is 5.75 τ and the aspect ratio is 5.75 τ/w_{coil}. Therefore, the aspect ratio of the quadruple receiver extended from the proposed dual receiver is 17.4% lower than that of the conventional quadruple-DD receiver. In summary, when the proposed receiver is extended as multiple receivers, it still has the advantage in reducing the aspect ratio.

III. Design of the Proposed Receiver

In the proposed receiver, the structure of the full-pitch coils is fixed by the pole pitch τ. However, as for the mixed-pitch coils, except the external overall size, the symmetry of the coils, the size and the numbers of turns of coil_1, coil_2, and coil_3 are all designable. These parameters affect the mutual inductance between the transmitter coil and the mixed-pitch coils and the cross coupling between the receiver coils. Therefore, the mixed-pitch coils are the key in the design of the proposed receiver. This section first gives the design method of the mixed-pitch coils, then analyzes the loss and efficiency of the system, and finally explores the influence of vehicle chassis on the magnetic coupler.

A. Structural Symmetry of the Mixed-Pitch Coils

According to the lengths of coil_1 and coil_3, the mixed-pitch coils can be divided into symmetrical and asymmetrical structures. When the lengths of coil_1 and coil_3 are the same, the structure of mixed-pitch coils is symmetrical, as shown in Fig. 2(b). The rms values of the induced voltages in the two sets of coils (U_{full} and U_{mixed}) are maintained at a spatial phase difference of 90° so that the lowest output fluctuation can be obtained. In addition, coil_2 is orthogonal to the full-pitch coils, so that there is no cross coupling between full-pitch and mixed-pitch coils.

When the lengths of coil_1 and coil_3 are not the same, the structure of mixed-pitch coils is asymmetrical. The asymmetric structure affects the output fluctuation factor and cross coupling between the receiver coils.

Fig. 10(a) shows the schematic diagram of the proposed receiver when electrical angles of coil_1, coil_2, and coil_3 are 80°, 150°, and 130°, respectively. Phasor diagrams of U_{full} and U_{mixed} are shown in Fig. 10(b).

In the asymmetric mixed-pitch coils, the rms values of induced voltages in coil_1 and coil_3 (denoted as U_α and U_γ) are not the same and their phase differences with the rms value of coil_2 (denoted as U_β) are not the same any more (see Fig. 10). Therefore, the amplitude of the induced voltage U_{mixed} in the mixed-pitch coils decreases and U_{full} and U_{mixed} cannot maintain a spatial phase difference of 90°along the driving direction any more.

In the asymmetric receiver shown in Fig. 10(a), the relationship between the output voltage after rectification and the receiver position x is shown in Fig. 10(c). In the symmetrical structure, the output voltage fluctuations $\triangle U\%$ is 29%. In the

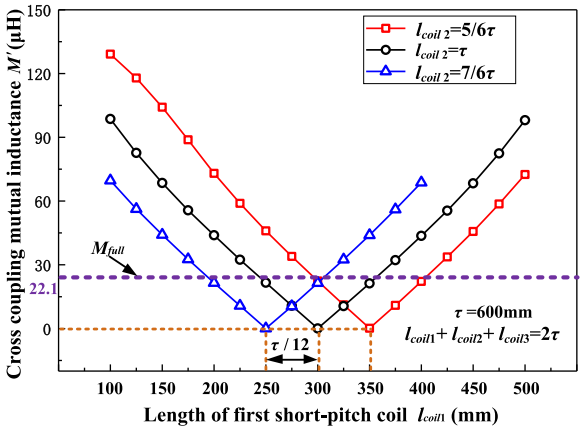

Fig. 11. Cross-coupling mutual inductance between full-pitch and mixed-pitch receiver coils versus the length of the first short-pitch coil in the mixed-pitch coils (l_{coil1}).

asymmetrical structure, $\triangle U\%$ of series and parallel connection modes are 47.6% and 46%, respectively. Thus, the asymmetric structure can increase the fluctuation factor of the output voltage.

The influence of the mixed-pitch coils' structural symmetry on the cross coupling between the receiver coils was explored by finite element simulation.

In simulation models, the total length of the receiver coils is kept constant at 2 τ. Except for the length of each coil in the mixed-pitch coils, other parameters remain unchanged, as listed in Table II. The asymmetry of the mixed-pitch coils can be adjusted by changing the lengths of coil_1, coil_2, and coil_3. The cross-coupling mutual inductance M' between full-pitch and mixed-pitch coils is shown in Fig. 11.

The simulation results in Fig. 11 are summarized in the following. First, the cross coupling between the full-pitch and the mixed-pitch coils is only affected by the symmetry of the mixed-pitch coils. The worse the coils' symmetry is, the larger the cross-coupling mutual inductance is. Unless the mixed-pitch coils are symmetrical, the cross coupling between two sets of coils cannot be zero. Second, when the lengths of coil_1 and coil_3 are the same, the length of coil_2 does not affect the cross coupling between two sets of coils. Therefore, it is not necessary to consider the cross coupling in the design of the size of coil_2.

The coupling coefficient k between the transmitter coil and mixed-pitch coils and the quality factor Q_{mixed} of the mixed-pitch coils are, respectively, defined as follows:

$$k = \frac{M_{\mathrm{mixed}}}{\sqrt{L_p \cdot L_{s-\mathrm{mixed}}}} \tag{15}$$

$$Q_{\mathrm{mixed}} = \frac{\omega \cdot L_{s-\mathrm{mixed}}}{r_{s-\mathrm{mixed}}}. \tag{16}$$

In the same way, the relationship between the two parameters defined above (quality factor Q_{mixed} and the coupling coefficient k) and the length of coil_1 (denoted as l_{coil1}) can be obtained by finite element simulation (see Fig. 12).

The simulation results in Fig. 12 are summarized in the following. First, when the length of coil_2 (denoted as l_{coil2}) is fixed, coupling coefficient k and quality factor Q_{mixed} are affected by the mixed-pitch coils' symmetry. Unless the mixed-pitch coils are symmetrical, k or Q_{mixed} cannot reach their maximum values. Second, the length of coil_2 (l_{coil2}) affects the maximum values of k and Q_{mixed}. When $l_{\mathrm{coil2}} = \tau$, the mixed-pitch receiver coils have the maximum coupling coefficient.

Similarly, the numbers of turns of coil_1 and coil_3 should be the same in order to ensure the symmetry of the mixed-pitch coils. Since the analysis process is basically the same, it will not be described here.

In summary, compared to the symmetrical mixed-pitch coils, the asymmetric structure has four disadvantages of large output fluctuation factor, cross coupling, low coupling coefficient k and low quality factor Q_{mixed}. Therefore, it is necessary to ensure the symmetrical mixed-pitch coils in the design of the proposed receiver.

B. Size Design of the Mixed-Pitch Coils

After completing the structural symmetry design of the mixed-pitch coils, the induced voltages U_{full} and U_{mixed} in the two sets of coils are always maintained at a phase difference of 90° along the driving direction. Then, the designed size and number of turns of coils in the two sets of coils should ensure that the amplitudes of U_{full} and U_{mixed} are the same so that the proposed receiver has the lowest output fluctuation factor.

Based on the simulation model listed in Table II, the coil width is changed for the simulation. As the coil width increases, the mutual inductance and coupling coefficient between the transmitter and receiver coils increases. When the coil width w_{coil} reaches $4\tau/3$, the coupling coefficient k reaches the maximum. Therefore, the receiver coil width is determined as $4\tau/3$.

Similarly, through changing the length of each coil in the simulation models, the relationship between mutual inductance amplitude and coil length is explored. The simulation results are shown in Fig. 13. It is worth noting that since coils coil_1 and coil_3 are of the same length, the mutual inductance magnitudes between the transmitter coil and the two coils are the same.

The simulation results in Fig. 13 are summarized in the following. First, with the increase in the receiver coil's length, the mutual inductance increases first and then decreases. If the wire diameter is ignored, the mutual inductance reaches the maximum value when the length of the receiver coil is equal to the pole pitch τ. Second, the mutual inductance is affected by the relative positions of the receiver coil and the receiver core. When the coil is located at the middle of the core, the mutual inductance amplitude (12.42 μH) is 112% of that when the coil is located at the side of the core (11.10 μH).

The above results may be interpreted as follows. When the N-type power supply rail is energized, equivalent magnetic poles of alternating N and S are generated along the driving direction, and the spacing between adjacent poles is τ. Along the driving direction, the magnetic field is in the same direction within the distance of $\pm 0.5\ \tau$ above the magnetic pole. Therefore, when the length of the receiver coil increases from 0 to τ, the magnetic flux passing through the receiver coil increases and the mutual inductance gradually increases and reaches the maximum when $l_{\mathrm{coil}} = \tau$. When the coil length is longer than the pole pitch τ,

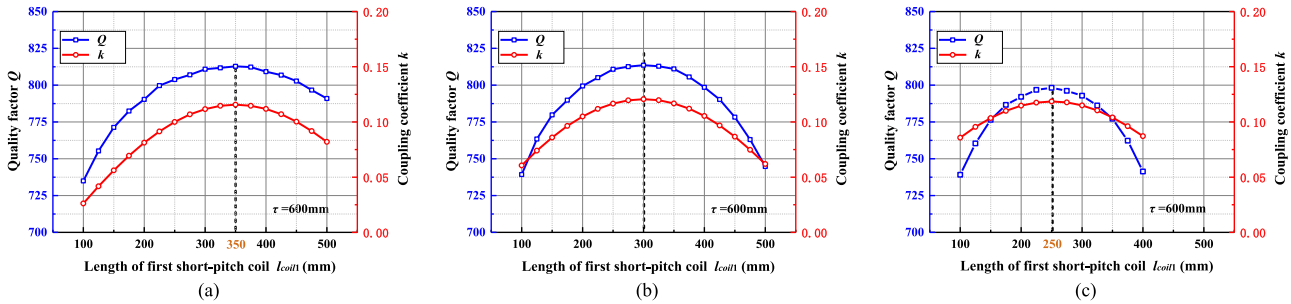

Fig. 12. Quality factor and coupling coefficient of the mixed-pitch coils versus the length of the first short-pitch coil when (a) $l_{\mathrm{coil2}} = 5/6\tau$, (b) $l_{\mathrm{coil2}} = \tau$, and (c) $l_{\mathrm{coil2}} = 7/6\tau$.

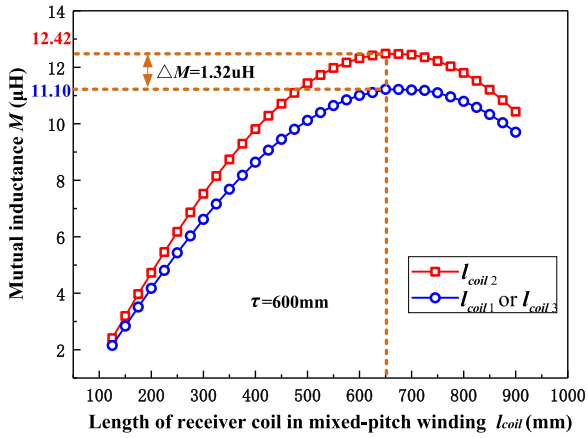

Fig. 13. Mutual inductance versus length of single receiver coil (l_{coil}).

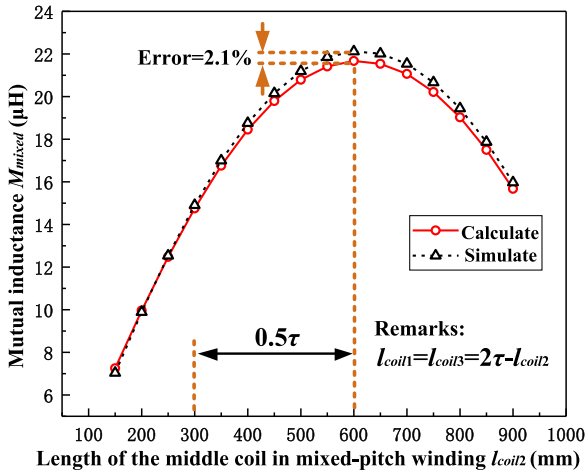

Fig. 14. Mutual inductance versus the length of the middle coil in the mixed-pitch coils (l_{coil2}).

one part of the magnetic flux passing through the coil is in the opposite directions and will offset partial flux, so that the net coupling magnetic flux and the mutual inductance decrease. Since the length of the receiver core is limited, the mutual inductance amplitude is related to the relative positions of the receiver coil and the receiver core. When the receiver coil is located on the side of the core, the mutual inductance decreases due to the core end effect.

To ensure the symmetry of the mixed-pitch coils, the length and turns of coil_1 and coil_3 are the same. In the design of the length of each receiver coil in the mixed-pitch coils, it is necessary to discuss whether the number of turns of the coil_2 (denoted as N_β) and the number of turns of coil_1 and coil_3 (denoted as N_α) are the same. When the turns of all the three coils are equal ($N_\alpha = N_\beta$), the total amount of wire l_{wire} of the mixed-pitch coils is independent of the length ratio of each coil. By substituting the mutual inductance amplitudes of coil_1, coil_2, and coil_3 shown in Fig. 13 into (6), the mutual inductance between the transmitter coil and the mixed-pitch coils can be calculated. The calculation and simulation results with different lengths of the coil_2 (l_{coil2}) are shown in Fig. 14. Since the total length of the mixed-pitch coils is 2τ, (4) indicates that the length of each coil in the mixed-pitch coils satisfies the following equation:

$$l_{\mathrm{coil1}} = l_{\mathrm{coil3}} = 2\tau - l_{\mathrm{coil2}}. \tag{17}$$

As shown in Fig. 14, the maximum error between the mutual inductances, calculated by (6) and obtained from the finite element simulation, is only 2.1%, thus verifying the theoretical analysis in Section II. Theoretical calculations and simulation results both show that when the numbers of turns of coil_1, coil_2, and coil_3 are the same, the mutual inductance between the transmitter coil and the mixed-pitch coils increases first and then decreases with the increase in l_{coil2}. When the length of coils satisfies the following equations: $l_{\mathrm{coil1}} = l_{\mathrm{coil3}} = 0.5\,\tau$ and $l_{\mathrm{coil2}} = \tau$, the mutual inductance reaches its maximum value.

When the numbers of turns of coils are not the same ($N_\alpha \neq N_\beta$), the total amount of wire in the mixed-pitch coils (l_{wire}) is related to the length of each coil. When the diameter of coil is ignored, l_{wire} satisfies the following equation:

$$l_{\mathrm{wire}} = 4N_\alpha \cdot (l_{\mathrm{coil1}} + w_{\mathrm{coil}}) + 2N_\beta \cdot (l_{\mathrm{coil2}} + w_{\mathrm{coil}}). \tag{18}$$

Then, the mutual inductance between the transmitter coil and the mixed-pitch coils is

$$M_{\mathrm{mixed-max}} = 2N_\alpha M_{\alpha-\max} \cdot \cos\frac{\alpha}{2} + N_\beta M_{\beta-\max}. \tag{19}$$

It is difficult to obtain the influence of coil turns on the system from (18) and (19), so we use the increments of the mutual inductance and wire amount in the analysis. When the numbers

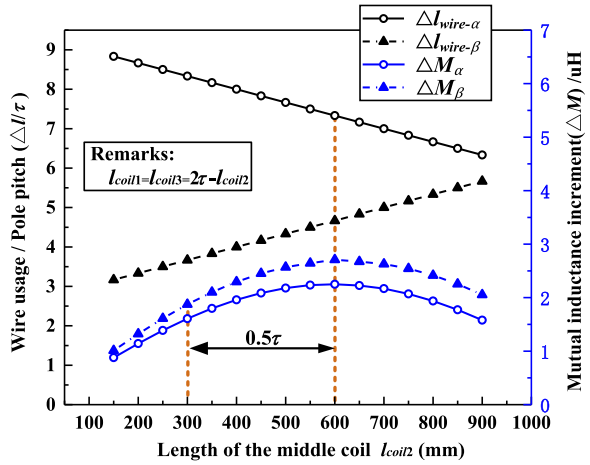

Fig. 15. Increments of mutual inductance (ΔM) and wire amount (Δl) versus the length of the middle coil in the mixed-pitch coils (l_{coil2}).

of turns of coil_1, coil_2, and coil_3 are, respectively, increased by only one turn, the increments of wire amount (denoted as $\Delta l_{\mathrm{wire}-\beta}$ and $\Delta l_{\mathrm{wire}-\alpha}$) are expressed as

$$\begin{cases} \Delta l_{\mathrm{wire}-\beta} = 2 \cdot (l_{\mathrm{coil2}} + w_{\mathrm{coil}}) \\ \Delta l_{\mathrm{wire}-\alpha} = 4 \cdot (l_{\mathrm{coil1}} + w_{\mathrm{coil}}). \end{cases} \tag{20}$$

The increments of the mutual inductance between the transmitter coil and the mixed-pitch coils (denoted as ΔM_α and ΔM_β) are expressed as

$$\begin{cases} \Delta M_\alpha = 2M_{a-\max} \cdot \cos\left(\frac{\alpha}{2}\right) \\ \Delta M_\beta = M_{\beta-\max}. \end{cases} \tag{21}$$

When $w_{\mathrm{coil}} = 4\tau/3$, according to (20) and (21), the relationships between $\Delta l_{\mathrm{wire}-\beta}$, $\Delta l_{\mathrm{wire}-\alpha}$, ΔM_β, and ΔM_α are obtained (see Fig. 15).

The results in Fig. 15 are summarized in the following. First, with the increase in l_{coil2}, $\Delta l_{\mathrm{wire}-\beta}$ increases linearly, but $\Delta l_{\mathrm{wire}-\alpha}$ decreases linearly ($\Delta l_{\mathrm{wire}-\alpha}$ is always greater than $\Delta l_{\mathrm{wire}-\beta}$). Second, the increments of mutual inductances (ΔM_β and ΔM_α) increase first and then decrease with the increase in l_{coil2}, and it reaches its maximum value when $l_{\mathrm{coil2}} = \tau$.

Therefore, when $l_{\mathrm{coil2}} = \tau$, the mutual inductance increment can be maximized with the less increment of wire amount. Therefore, in the design, the size of each coil should satisfy the following equation:

$$l_{\mathrm{coil1}} = l_{\mathrm{coil3}} = 0.5\tau, \quad l_{\mathrm{coil2}} = \tau. \tag{22}$$

In summary, the length of each coil in the mixed-pitch coils should satisfy (22) and the number of turns of each coil should be specifically designed according to the output power requirements.

C. Effieciency and Loss Calculation

Efficiency is an important index in the DWC system for EV. The ratio of output power P_o to inverter output power P_{in} is defined as ac–dc efficiency (denoted as $\eta_{\mathrm{AC-DC}}$) and it satisfies the following equation:

$$\eta_{\mathrm{AC-DC}} = \frac{P_o}{P_{\mathrm{in}}} = \frac{P_o}{P_o + P_{\mathrm{Cu}} + P_{\mathrm{Fe}} + P_{\mathrm{Cap}} + P_{\mathrm{rectifier}}} \tag{23}$$

where P_{Cu} indicates the copper loss of coils, P_{Fe} indicates the core loss in ferrite, P_{Cap} indicates the capacitor loss, and $P_{\mathrm{rectifier}}$ indicates the receiver rectifier loss.

The copper loss P_{Cu} includes two parts: the loss caused by skin effect (denoted as P_{skin}), and the loss caused by proximity effect (denoted as P_{prox}) [20]

$$P_{\mathrm{Cu}} = P_{\mathrm{skin}} + P_{\mathrm{prox}}. \tag{24}$$

The loss caused by skin effect can be calculated as [21]

$$P_{\mathrm{skin}} = n \cdot R_{\mathrm{dc}} \cdot F_R(f_0) \cdot \left(\frac{\hat{I}}{n}\right)^2 \cdot l_{\mathrm{wire}} \tag{25}$$

where n is the number of strands of Litz wire, R_{dc} is the dc resistance per unit length of a single strand, $\hat{I}$ is the current peak value, and $F_R(f_0)$ is a function of current frequency [21].

The loss caused by the proximity effect can be calculated as

$$\begin{aligned} P_{\mathrm{prox}} &= P_{\mathrm{prox},e} + P_{\mathrm{prox},i} \\ &= \oint n \cdot R_{\mathrm{dc}} \cdot G_R(f) \cdot \left(\hat{H}_e^2 + \frac{\hat{I}^2}{2\pi^2 d_a^2}\right) dl_{\mathrm{wire}} \end{aligned} \tag{26}$$

where $G_R(f)$ is another function of current frequency, $\hat{H}_e$ is the magnetic field strength passing through the conductor, and d_a is the outer diameter of the overall Litz wire. The loss caused by the proximity effect can be divided into two parts: the loss caused by the internal magnetic field strength of the neighboring strands (denoted as $P_{\mathrm{prox},i}$), and the loss caused by the external magnetic field strength (denoted as $P_{\mathrm{prox},e}$). $P_{\mathrm{prox},e}$ can be obtained by integrating the magnetic field strength $\hat{H}_e$ passing through the conductor along the path of each coil with the aid of the finite element simulation software.

The loss of ferrite core can be calculated with the Steinmetz equation [20], [22]

$$P_{\mathrm{Fe}} = \iiint K_h \cdot f^\alpha \cdot B^\beta dx dy dz \tag{27}$$

where K_h, α, and β are called Steinmetz coefficients and can be calculated from the BP curve provided by the manufacturer. The ferrite core used in this article is PC95 ferrite produced by TDK Company. For this material, the Steinmetz coefficients are calculated as follows: $K_h = 0.5189$, $\alpha = 1.5$, and $\beta = 2.44$.

Capacitor loss P_{Cap} can be calculated with its equivalent internal resistance. In this article, the equivalent internal resistance of the resonant capacitor was measured at the working frequency with an impedance analyzer.

The loss of rectifier $P_{\mathrm{rectifier}}$ can be obtained by the experimental measurement or circuit simulation.

D. Influence of the Vehicle Chassis on a Magnetic Coupler

The vehicle chassis is usually made of ferromagnetic materials such as steel plate, which has high relative permeability [23],

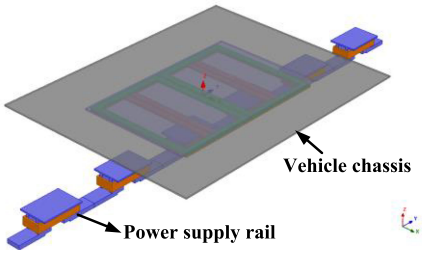

Fig. 16. Simulation model of the magnetic coupler with vehicle chassis.

TABLE III
SIMULATION RESULTS OF MAGNETIC COUPLER'S SELF-INDUCTANCE AND MUTUAL INDUCTANCE WITH OR WITHOUT VEHICLE CHASSIS

	$M_{full\text{-}max}$(μH)	$M_{mixed\text{-}max}$(μH)	$L_{s\text{-}full}$(μH)	$L_{s\text{-}mixed}$(μH)	L_p(μH)
Without chassis	22.26	22.01	174.0	181.9	180.4
With chassis	22.45	22.03	175.7	182.3	181.5
Change	+0.85%	+0.09%	+0.97%	+0.22%	+0.61%

[24]. In engineering applications, it may affect the magnetic field distribution of the magnetic coupler [25], [26]. In order to reduce the influence of metal chassis, a flat receiver core is adopted in the proposed receiver for shielding.

The influence of metal chassis on magnetic coupler is analyzed by finite element simulation. The simulation model is shown in Fig. 16. The high-quality carbon structural steel 1010 (2000 mm × 1500 mm × 10 mm) is used to replace the vehicle chassis and the distance between the steel plate and the receiver core is 3 cm. The parameters of the magnetic coupler are kept unchanged.

Table III gives the simulation results of mutual inductance and self-inductance of the transmitter coil and receiver coils with or without the metal chassis.

The simulation results show that the mutual inductance or self-inductance of the transmitter coil and receiver coils has not been changed even though the influence of the vehicle chassis is considered. The result verifies that the flat receiver core can well shield the magnetic field of the magnetic coupler. The vehicle chassis has little influence on the performance of the magnetic coupler.

IV. EXPERIMENTAL EVALUATION

A. Prototype System

To verify the advantages of the proposed receiver, an experiment prototype shown in Fig. 17 was built. The transmitter of the prototype used an N-type power supply rail with a total length of 3.6 m. The widths of the full-pitch and the mixed-pitch coils are both $4\tau/3$ (800 mm) and the total length is 2τ (1200 mm). The length of each coil in the mixed-pitch receiver coils satisfies that: $l_{\text{coil1}} = l_{\text{coil3}} = 300$ mm, $l_{\text{coil2}} = 600$ mm. The air gap of the magnetic coupler was 20 cm and the operating frequency was selected to 20 kHz due to the inverter. All the other parameters of the prototype are listed in Table II. In the prototype, full-pitch and mixed-pitch coils were connected in series after rectification and the battery load was simulated by using a water tank resistance of 12.3 Ω. The equivalent circuit of the system is shown in Fig. 3(a).

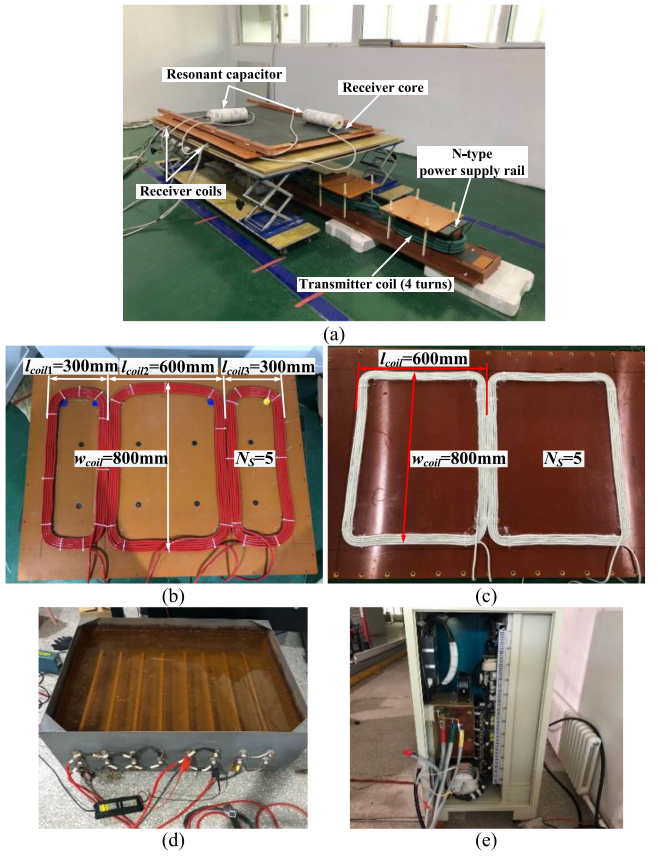

Fig. 17. Experimental prototype. (a) Overall view of the experimental prototype. (b) Mixed-pitch receiver coils. (c) Full-pitch receiver coils. (d) Resistance load. (e) High-frequency inverter.

TABLE IV
MEASURED PARAMETERS OF THE PROTOTYPE

Parameters	Symbols	Values	Units
Inductance of transmitter coil	L_p	174.1	μH
Inductance of the two sets of receiver coils	$L_{s\text{-}full}$ $L_{s\text{-}mixed}$	147.3 190.1	μH
Internal resistance of transmitter	r_p	78.4	mΩ
Internal resistance of the two sets of receivers	$r_{s\text{-}full}$ $r_{s\text{-}mixed}$	55.9 67.6	mΩ
Resonant capacitor of transmitter coil	C_p	0.36	μF
Resonant capacitor of the two sets of receiver coils	$C_{s\text{-}full}$ $C_{s\text{-}mixed}$	0.43 0.33	μF
Mutual inductance between transmitter coil and receiver coils	$M_{full\text{-}max}$ $M_{mixed\text{-}max}$	21.8 21.7	μH
Cross coupling between receiver coils	M'	2.0	μH

The parameters of the prototype (see Table IV) were measured by an impedance analyzer.

From the measurement results listed in Table IV, it can be seen that there is almost no cross coupling between full-pitch and mixed-pitch coils in the prototype. Therefore, the symmetrical mixed-pitch coils can eliminate cross coupling between the two sets of receiver coils. The measured value of mutual inductance between two sets of coils is 2 μH since the fabrication error in the fabrication process of the experimental prototype makes coil_1 and coil_3 are not completely symmetrical.

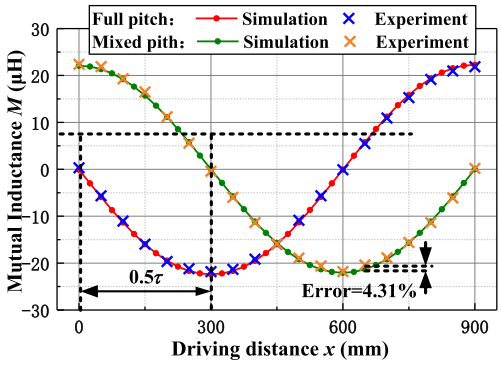

(a)

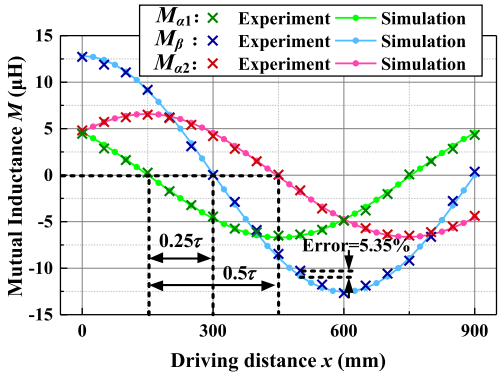

(b)

Fig. 18. Measured mutual inductance. (a) Mutual inductance between the transmitter coil and the receiver coils. (b) Mutual inductance between the transmitter coil and three receiver coils in the mixed-pitch coils.

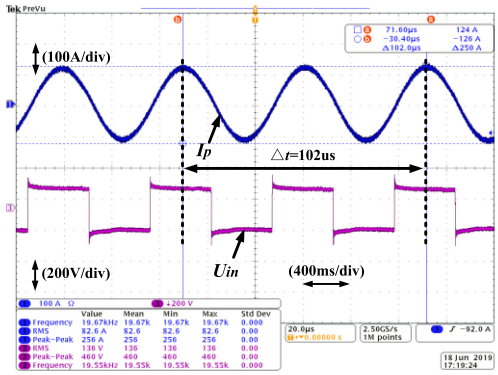

Fig. 19. Waveforms of inverter's output voltage and the transmitter current.

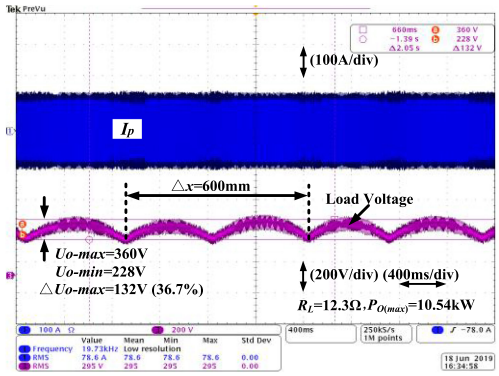

Fig. 20. Waveforms of load voltage and transmitter current during the DWC process.

B. Measurments of Mutual Inductance

When the receiver moved along the driving direction, the mutual inductance between the transmitter coil and receiver coils was measured with an impedance analyzer. The measurement and simulation results are shown in Fig. 18.

The measured M_{full}–x curve and the M_{mixed}–x curve were approximately coincident with the simulation results with the maximum error of 4.31% (see Fig. 18). The result proved the accuracy of the finite element simulation. During the movement of the receiver, M_{full} and M_{mixed} varied sinusoidally with x and maintained a phase difference of 90° along the driving direction. Besides, the amplitudes of them were the same. For the M_{coil1}–x, M_{coil2}–x, and M_{coil3}–x curves, the maximum error between the measured and simulation results was 5.35%. M_{coil1} and M_{coil3} had the same amplitudes and maintained a phase difference of ±45° with M_{coil2} along the driving direction, respectively. In summary, the measured mutual inductance shown in Fig. 18 was consistent with the theoretical analysis, thus proving the working principle analysis in Section II.

C. Output Voltage Fluctuation

The high-frequency inverter used in the experiment shown in Fig. 17(e) adopted insulated gate bipolar transistor (IGBT) devices and the constant-current control method. When the system was working, the waveforms of the inverter output voltage and the transmitter coil current were obtained (see Fig. 19).

To verify whether the proposed receiver can effectively reduce the output fluctuation factor, the output voltage across the load was measured during the movement of the receiver. Fig. 20 shows the waveforms of the load voltage and the transmitter coil current during the movement of the receiver.

The maximum output power was 10.54 kW during the movement of the receiver (see Fig. 20). The load voltage periodically fluctuated with the change in the position of the receiver. The maximum and minimum values were, respectively, 360 and 228 V and the output fluctuation factor was 36.7%. The experimental results were consistent with the theoretical analysis in Section II, verifying that the dual mixed-pitch receiver could effectively reduce the output fluctuation under the premise of ensuring a low aspect ratio.

The experimental results showed that the measured output fluctuation factor was slightly larger than the theoretical value (29%). The difference might be interpreted as follows. First, it was necessary to move the receiver of the prototype manually, so the receiver inevitably had the lateral displacement during the movement and the minimum value of the output voltage was decreased. Second, due to the fabrication error in the fabrication process of the prototype, there is a small cross-coupling mutual inductance between the two sets of receiver coils. Therefore, the output fluctuation factor increases.

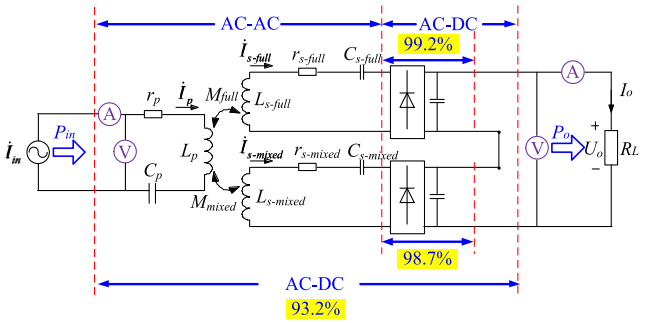

Fig. 21. System efficiency measurement ($R_L = 12.3\ \Omega$).

D. Efficiency and Loss Analysis

Since the core loss of the magnetic coupler could not be measured directly, the ac–dc efficiency $\eta_{\text{AC-DC}}$ of the system was measured in the article. In the experiment, the rms value of the transmitter current I_p was kept constant at 80 A. When the receiver moved to the position with the highest output voltage, the measured output power P_o of the system was 10.25 kW and the measured input power of the magnetic coupler P_{in} was 10.99 kW. The efficiency measurement results of each part are shown in Fig. 21.

The measured ac–dc efficiency $\eta_{\text{AC-DC}}$ of the system was 93.2% and the efficiencies of the rectifiers connected with the full-pitch coils and the mixed-pitch coils were, respectively, 99.2% and 98.7%.

The total loss of the system except the inverter was measured to be 745 W and the losses of the two rectifiers were, respectively, 44.2 and 66.76 W. In the prototype, the measured internal resistances of the resonant capacitance in the transmitter, the full-pitch receiver, and the mixed-pitch receiver at 20 kHz were 29.6, 24.7, and 34.6 mΩ, respectively. However, the calculated loss was 657.3 W (–11.8%), which was slightly less than the measurement result because the eddy current losses in receiver lifting device or connecting cable lugs were not considered in the calculation process.

Fig. 22(a) shows the proportion of the calculated loss of each part. The capacitor loss P_{Cap} accounted for the highest proportion (38.5%) of all losses, followed by the core loss (21.46%). The result might be interpreted as follows. The high-power WPT system required the high voltage withstand level for the resonant capacitor, so the capacitor usually adopted the multiple series connection mode to increase the voltage withstand level. Therefore, the equivalent internal resistance of the capacitor increases.

Fig. 22(b) shows the calculation results of the copper loss P_{Cu} in the coils. Due to the large current in the transmitter coil, the copper loss in the transmitter coil was significantly greater than that of the two sets of receiver coils. The loss caused by skin effect (P_{skin}) accounts for the main proportion, followed by the external proximity effect loss $P_{\text{prox},e}$. The internal proximity effect losses $P_{\text{prox},i}$ was so small that it could be ignored.

Fig. 22(c) shows the calculation results of the losses of resonant capacitors P_{Cap} in transmitter and receiver. The losses generated by the capacitor of the transmitter (C_p), the capacitor of the full-pitch receiver $(C_{s-\text{full}})$ and the capacitor of the mixed-pitch receiver $(C_{s-\text{mixed}})$ were 189.4, 26.1, and 36.6 W, respectively. The loss of the resonant capacitor in the transmitter was much greater than that in both receivers.

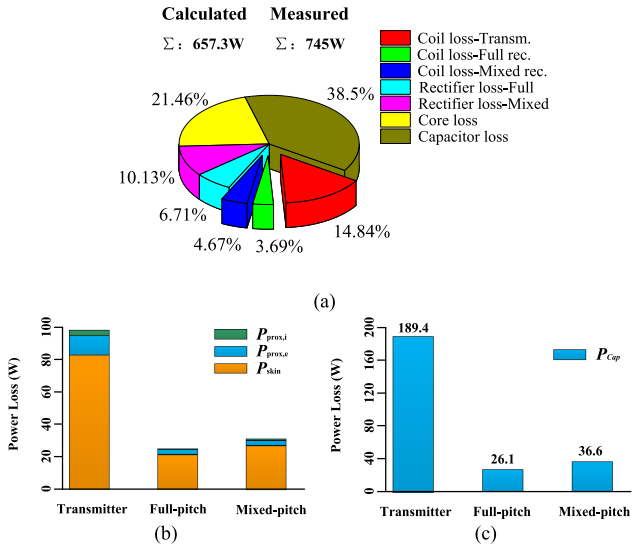

Fig. 22. (a) Calculated loss components contributing to the total losses of the prototype at an output power of 10.25 kW. (b) Calculated copper loss components in the transmitter coils and receiver coils. (c) Calculated capacitor loss components in the transmitter and receivers.

V. Conclusion

This article proposes a dual-layer receiver with a low aspect ratio for EV wireless power transfer system. It solves the main problem of conventional DD receiver coils when it is mated with the power supply rails with alternate magnetic poles, the sinusoidal fluctuation of the output power. In addition, it avoided the disadvantages of high aspect ratio, limited installation space and interphase coupling in the conventional dual-DD-type receiver. Theoretically, simulation and experimental results proved that compared with a conventional receiver, the proposed receiver could reduce the aspect ratio by 20% with the same output fluctuation factor and eliminate cross coupling between the receiver coils. The experimental results showed that the output fluctuation factor of the proposed receiver could be reduced to 36.7% with the maximum output power of 10.54 kW and ac–dc efficiency of 93.2%.

In the dual-layer receiver, the mixed-pitch coils are the key in the design. The coils must be symmetrical in order to eliminate cross coupling between full-pitch and mixed-pitch coils. When the length of each coil in the mixed-pitch coils satisfies the following equations: $l_{\text{coil1}} = l_{\text{coil3}} = 0.5\ \tau$ and $l_{\text{coil2}} = \tau$, the mutual inductance between the transmitter coil and receiver coils reaches the maximum value and the amount of wire used in the receiver is the least. The flat receiver core can well shield the magnetic field of the magnetic coupler, so the vehicle chassis has almost no influence on the performance of the system.

For the vehicles with a large chassis installation space, the proposed receiver can be extended to multiple receivers through multiple connections so as to further reduce the output fluctuation factor. Compared with the conventional multiple receivers

extended from dual-DD receivers, the new multiple receivers can lower the aspect ratio and eliminate cross coupling between receiver coils with the same output fluctuation factor.

REFERENCES

[1] M. Yilmaz and P. T. Krein, "Review of battery charger topologies, charging power levels, and infrastructure for plug-in electric and hybrid vehicles," *IEEE Trans. Power Electron.*, vol. 28, no. 5, pp. 2151–2169, May 2013.

[2] S. Y. Choi, B. W. Gu, S. Y. Jeong, and C. T. Rim, "Advances in wireless power transfer systems for roadway-powered electric vehicles," *IEEE J. Emerg. Sel. Topics Power Electron.*, vol. 3, no. 1, pp. 18–36, Mar. 2015.

[3] C. C. Mi, G. Buja, S. Y. Choi, and C. T. Rim, "Modern advances in wireless power transfer systems for roadway powered electric vehicles," *IEEE Trans. Ind. Electron.*, vol. 63, no. 10, pp. 6533–6545, Oct. 2016.

[4] G. A. Covic and J. T. Boys, "Modern trends in inductive power transfer for transportation applications," *IEEE J. Emerg. Sel. Topics Power Electron.*, vol. 1, no. 1, pp. 28–41, Mar. 2013.

[5] Z. Zhao, F. Liu, and K. Chen, "New progress of wireless charging technology for electric vehicles," *Trans. China Electrotech. Soc.*, vol. 31, pp. 30–40, 2016.

[6] J. Huh, S. W. Lee, W. Y. Lee, G. H. Cho, and C. T. Rim, "Narrow-width inductive power transfer system for online electrical vehicles," *IEEE Trans. Power Electron.*, vol. 26, no. 12, pp. 3666–3679, Dec. 2011.

[7] S. Y. Choi, S. Y. Jeong, B. W. Gu, G. C. Lim, and C. T. Rim, "Ultraslim S-type power supply rails for roadway-powered electric vehicles generalized models on self-decoupled dual pick-up coils for a large lateral tolerance," *IEEE Trans. Power Electron.*, vol. 30, no. 11, pp. 6456–6468, Nov. 2015.

[8] Z. Wang *et al.*, "A novel magnetic coupling mechanism for dynamic wireless charging system for electric vehicles," *IEEE Trans. Veh. Technol.*, vol. 67, no. 1, pp. 124–133, Jan. 2018.

[9] J. Jiang., C. Zhu, K. Song, G. Wei, and Q. Zhang, "Novel power receiver for dynamic wireless power transfer system," in *Proc. 41st Annu. Conf. IEEE Ind. Electron. Soc.*, 2015, pp. 2247–2251.

[10] S. Cui, Z. Wang, S. Han, C. Zhu, and C. C. Chan, "Analysis and design of multiphase receiver with reduction of output fluctuation for EV dynamic wireless charging system," *IEEE Trans. Power Electron.*, vol. 34, no. 5, pp. 4112–4124, May 2019.

[11] S. Cui, B. Song, X. Gao, and S. Dong, "A narrow-width three phase magnetic coupling mechanism with constant output power for electric vehicles dynamic wireless charging," in *Proc. IEEE PELS Workshop Emerg. Technol., Wireless Power Transfer*, 2018, pp. 1–6.

[12] H. Li, Y. Liu, K. Zhou, Z. He, W. Li, and R. Mai, "Uniform power IPT system with three-phase transmitter and bipolar receiver for dynamic charging," *IEEE Trans. Power Electron.*, vol. 34, no. 3, pp. 2013–2017, Mar. 2019.

[13] R. Mai, H. Li, Y. Liu, K. Zhou, L. Fu, and Z. He, "A three-phase dynamic wireless charging system with constant output voltage," *Energies*, vol. 11, no. 1, p. 45, Jan. 2018.

[14] G. A. Covic, J. T. Boys, M. L. G. Kissin, and H. G. Lu, "A three-phase inductive power transfer system for roadway-powered vehicles," *IEEE Trans. Ind. Electron.*, vol. 54, no. 6, pp. 3370–3378, Dec. 2007.

[15] C. Park, S. Lee, S. Y. Jeong, G. Cho, and C. T. Rim, "Uniform power I-type inductive power transfer system with DQ-power supply rails for on-line electric vehicles," *IEEE Trans. Power Electron.*, vol. 30, no. 11, pp. 6446–6455, Nov. 2015.

[16] G. R. Nagendra, G. A. Covic, and J. T. Boys, "Sizing of inductive power pads for dynamic charging of EVs on IPT highways," *IEEE Trans. Transp. Electrific.*, vol. 3, no. 2, pp. 405–417, Jun. 2017.

[17] Y. Li *et al.*, "A new coil structure and its optimization design with constant output voltage and constant output current for electric vehicle dynamic wireless charging," *IEEE Trans. Ind. Inform.*, vol. 15, no. 14, pp. 5244–5256, Sep. 2019.

[18] K. Song, C. Zhu, K. E. Koh, T. Imura, and Y. Hori, "Wireless power transfer for running EV powering using multi-parallel segmented rails," in *Proc. IEEE PELS Workshop Emerg. Technol., Wireless Power*, Daejeon, South Korea, 2015, pp. 1–6.

[19] M. L. G. Kissin, J. T. Boys, and G. A. Cvic, "Interphase mutual inductance in polyphase inductive power transfer systems," *IEEE Trans. Ind. Electron.*, vol. 56, no. 7, pp. 2393–2400, Jul. 2009.

[20] R. Bosshard, J. W. Kolar, J. Mühlethaler, I. Stevanovic, B. Wunsch, and F. Canales, "Modeling and –Pareto optimization of inductive power transfer coils for electric vehicles," *IEEE J. Emerg. Sel. Topics Power Electron.*, vol. 3, no. 1, pp. 50–64, Mar. 2015.

[21] J. Mühlethaler, "Modeling and multi-objective optimization of inductive power components," Ph.D. dissertation, Swiss Federal Inst. Technol. Zurich, ETH Zürich, Zürich, Switzerland, 2012.

[22] J. Muhlethaler, J. Biela, J. W. Kolar., and A. Ecklebe, "Core losses under the DC bias condition based on Steinmetz parameters," *IEEE Trans. Power Electron.*, vol. 27, no. 2, pp. 953–963, Feb. 2012.

[23] M. Ibrahim, L. Pichon, L. Bernard, A. Razek, J. Houivet, and O. Cayol, "Advanced modeling of a 2-kW series–series resonating inductive charger for real electric vehicle," *IEEE Trans. Veh. Technol.*, vol. 64, no. 2, pp. 421–430, Feb. 2015.

[24] M. Ibrahim *et al.*, "Inductive charger for electric vehicle: Advanced modeling and interoperability analysis," *IEEE Trans. Power Electron.*, vol. 31, no. 12, pp. 8096–8114, Dec. 2016.

[25] Q. Zhu, Y. Zhang, C. Liao, Y. Guo, L. Wang, and F. Li, "Experimental study on asymmetric wireless power transfer system for electric vehicle considering ferrous chassis," *IEEE Trans. Transp. Electrific.*, vol. 3, no. 2, pp. 427–433, Jun. 2017.

[26] W. Zhong, H. Cui, H. Li, A. U. Ibrahim, and D. Xu, "Study on the effect of ferrite layers in a wireless charging system with automotive chassis," in *Proc. IEEE Int. Power Electron. Appl. Conf. Expo.*, 2018, pp. 1–6.

Beibei Song was born in Henan Province, China. He received the B.S. and M.S. degrees in 2016 and 2018, respectively, from the School of Electrical Engineering and Automation, Harbin Institute of Technology, Harbin, China, where he is currently working toward Ph.D. degree.

His research interests include wireless power transfer and dynamic wireless charging for electric vehicles.

Shuai Dong was born in Shandong Province, China, in 1987. He received the M.S. and Ph.D. degrees in electrical engineering from the Harbin Institute of Technology (HIT), Harbin, China, in 2011 and 2016, respectively.

In 2017, he joined the Institute of Wireless Power Transfer Technology, HIT, where he is currently a Lecturer, and also, a Postdoctoral Researcher. His research interests include dynamic wireless power transfer technology, Z-source converters, and novel power electronics converter topologies for electric vehicle applications.

Yong Li was born in Heilongjiang Province, China, in 1964. He received the Ph.D. degree in electrical engineering from the Harbin Institute of Technology (HIT), Harbin, China, in 1988.

He is currently a Professor with the Department of Electrical Engineering, HIT. His research interests include Permanent-Magnet Synchronous Motors (PMSMs), special motors, and their applications.

Shumei Cui was born in Heilongjiang Province, China, on November 22, 1964. She received the Ph.D. degree in electrical engineering from the Harbin Institute of Technology (HIT), Harbin, China, in 1998.

She is currently a Professor with the Department of Electrical Engineering, HIT. Her research interests include the design and control of micro and special electric machines, electric drive system of electric vehicles, control and simulation of hybrid electric vehicles, and intelligent test and fault diagnostics of electric machines.

Dr. Cui is the Vice Director Member of the Micro and Special Electric Machine Committee and the Chinese Institute of Electronics, and a member of the Electric Vehicle Committee and the National Automotive Standardization Technical Committee.